The Company of Biologists

RESEARCH ARTICLE

Mon1–Ccz1 activates Rab7 only on late endosomes and dissociates from the lysosome in mammalian cells

Sayaka Yasuda[1], So Morishita[1], Akane Fujita[1], Tomohisa Nanao[1], Naoyuki Wada[2], Satoshi Waguri[3], Giampietro Schiavo[4], Mitsunori Fukuda[5] and Takeshi Nakamura[1,*]

ABSTRACT

Rab GTPases act as molecular switches regulating various aspects of membrane trafficking. Among them, Rab5 and Rab7 play central roles in the endolysosomal network. Although many effectors downstream of Rab7 have been elucidated, our present understanding of the mechanism regulating Rab7 activity is extremely limited. It has only recently been accepted that the Mon1–Ccz1 complex is a Rab7 guanine nucleotide exchange factor, but it still remains unclear what the location where Mon1–Ccz1 works with Rab7 is. To address what kind of change or switch exists in the regulatory mechanism upstream of Rab7 during its transition from the late endosome to lysosome, we examined Rab7 activity in steady-state cells and during EGF-induced macropinocytosis using a newly developed FRET sensor. A combination of a Rab7 sensor and confocal FRET imaging techniques revealed that the activation of Rab7 on late endosomes depends on Mon1–Ccz1 and is implicated in late-endosome–lysosome fusion. In contrast, Rab7 activity on lysosomes was independent of Mon1–Ccz1 and active Rab7 played a role in perinuclear clustering of lysosomes.

KEY WORDS: Small GTPase, FRET, Endolysosomal pathway, GEF

INTRODUCTION

Endocytosis and endolysosomal transport are linked to almost all aspects of cell life and diseases. The endocytic transport of proteins and lipids is initiated at the plasma membrane. Endocytosed vesicles fuse with early endosomes, which mature into late endosomes prior to their fusion with lysosomes. By sorting, processing, recycling, activating, and degrading incoming substances and receptors, endosomes are responsible for the regulation and fine tuning of numerous cellular pathways. Two Rab GTPases, Rab5 (of which there are three isoforms, A, B and C; here, the most-studied Rab5 protein, Rab5a, has been examined) and Rab7 (also known as Rab7a), are of key importance for the endolysosomal network (Huotari and Helenius, 2011; Stenmark, 2009). Rab5 functions at early endosomes, whereas Rab7 is required on late endosomes and lysosomes. The physiological importance of Rab7 in the endolysosomal system is well recognised in a wide range of cell types (Wartosch et al., 2015), and the molecular mechanisms

controlled by active Rab7 have been considerably elucidated (Nordmann et al., 2012). However, our understanding of the mechanism that regulates Rab7 activation is still extremely limited. In fact, it has only recently been accepted that the complex between Mon1 (which has two isoforms Mon1a and Mon1b) and Ccz1 is a guanine nucleotide exchange factor (GEF) for Rab7 in mammals (Gerondopoulos et al., 2012; Nordmann et al., 2010).

Despite much effort, the question as to where Mon1–Ccz1 interacts with Rab7 has not been completely addressed. This is partly because Mon1–Ccz1 is a versatile complex, which can play roles in Rab7 activation as a GEF (Nordmann et al., 2010), HOPS recruitment by direct binding (Poteryaev et al., 2010) and Rab7 recruitment to a membrane as a GDP dissociation inhibitor (GDI) displacement factor (GDF) (Kinchen and Ravichandran, 2010). Another difficulty is that there is only limited information known about when and where Rab7 is activated in the endolysosomal network. To determine whether Mon1–Ccz1 activates Rab7 either on late endosomes or lysosomes (or both), we used a novel Förster resonance energy transfer (FRET) biosensor.

In the present study, we found substantial variation in Rab7 activity on individual endosomes in steady-state cells, and a gradual increase in Rab7 activity on maturing macropinosomes. Using a novel Rab7 sensor and confocal FRET imaging techniques, we showed that Rab7 activity on late endosomes depended on Mon1–Ccz1, but that on lysosomes was independent of Mon1–Ccz1. In support of this finding, Ccz1 depletion did not change the perinuclear accumulation of lysosomes, whose position depends on active Rab7. Thus, we revealed that a switch mechanism exists upstream of Rab7 during the transition from the late endosome to the lysosome. This machinery might contribute to the unidirectionality in late-endosome-to-lysosome transition, as the Rab5-to-Rab7 conversion does during early-to-late endosome maturation (Poteryaev et al., 2010; Rink et al., 2005).

RESULTS

Development of a sensor for Rab7 activity

To visualise Rab7 activity in living cells, we developed a genetically encoded FRET sensor, termed Raichu-Rab7. The basic structure of Raichu-Rab7 was modified from that of a previously developed Rab5 sensor (Kitano et al., 2008) by introducing the Eevee backbone (Komatsu et al., 2011) with additional two linkers for improved function. The sensor comprised YPet-GL, the Rab7-binding domain of Rabring7, super-enhanced CFP and Rab7 (Fig. 1A).

Characterisation of Raichu-Rab7 was conducted similarly to that of other previously reported Raichu sensors (Kitano et al., 2008; Mochizuki et al., 2001). The GTP loading of the Rab7 sensors correlated well with that of the authentic Rab7 proteins (Fig. 1B), and the GTP loading obtained was similar to that previously reported using a GTP overlay assay (Spinosa et al., 2008).

[1]Division of Biosignaling, Research Institute for Biomedical Sciences, Tokyo University of Science, Noda, Chiba 278-0022, Japan. [2]Department of Applied Biological Science, Tokyo University of Science, Noda, Chiba 278-8510, Japan. [3]Department of Anatomy and Histology, Fukushima Medical University, Fukushima, Fukushima 960-1295, Japan. [4]UCL Institute of Neurology, University College London, Queen Square, London WC1N 3BG, UK. [5]Laboratory of Membrane Trafficking Mechanisms, Department of Developmental Biology and Neurosciences, Graduate School of Life Sciences, Tohoku University, Sendai, Miyagi 980-8578, Japan.
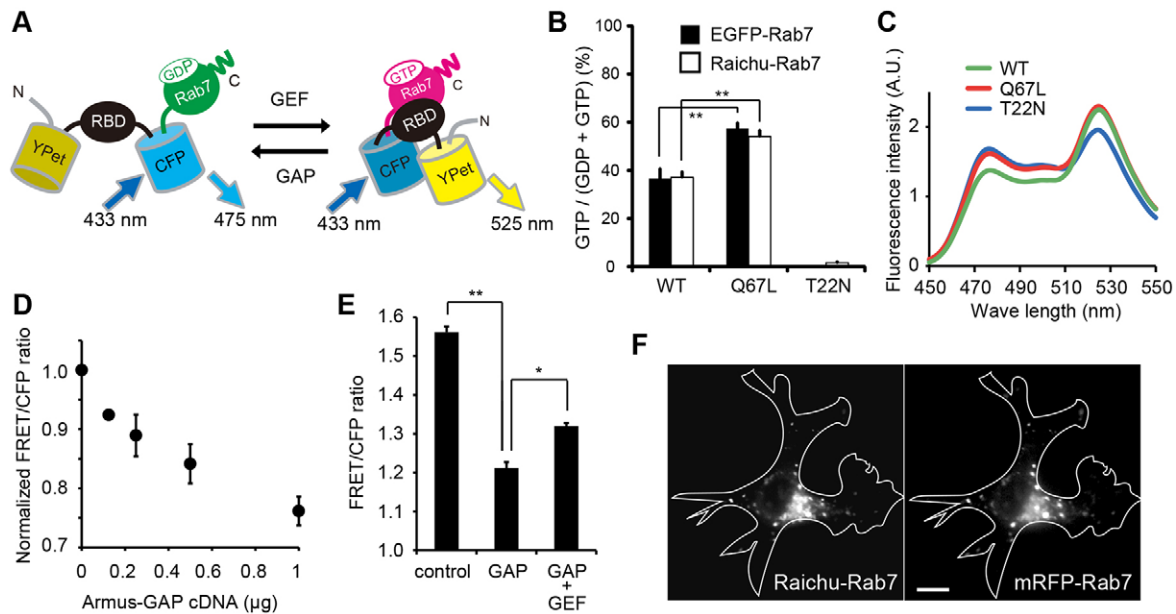
*Author for correspondence (tnakamr@rs.noda.tus.ac.jp)

Fig. 1. Basic properties of Raichu-Rab7. (A) Schematic representation of Raichu-Rab7 bound to GDP or GTP. YPet and CFP denote a yellow- and cyan-emitting mutant of GFP, respectively. RBD, GEF and GAP indicate the Rab7-binding domain of Rabring7, the guanine nucleotide exchange factor for Rab7 and the Rab7 GTPase-activating protein, respectively. (B) COS-7 cells expressing Raichu-Rab7 or EGFP–Rab7 were labelled with $^{32}P_i$. The guanine nucleotides bound to the GTPases were analysed by thin-layer chromatography, and the mean±s.e.m. of three samples is shown. **$P<0.01$ (one-way ANOVA followed by Dunnett's post-hoc test). (C) Emission spectra of Raichu-Rab7 (excited at 433 nm) expressed in 293-F cells. WT, Q67L and T22N denote the wild-type, constitutively active, and dominant negative mutants of Rab7, respectively. (D) Negative linear correlation between the ratio of FRET fluorescence intensity to CFP fluorescence intensity (FRET/CFP ratio) of Raichu-Rab7 and the extent of coexpression of the GAP domain of Armus. The FRET/CFP ratio was obtained from spectrograms of 293-F cells co-transfected with pRaichu-Rab7 and varying amounts of pCAGGS-Armus-GAP. Bars are s.e.m. (n=4). (E) pRaichu-Rab7 was co-transfected into 293-F cells with pCAGGS-Armus-GAP or the combination of pCAGGS-Armus-GAP, pEF-T7-Mon1a and pEF-T7-Ccz1. The FRET/CFP ratio was obtained as in D. The average of four samples is shown with s.e.m. *$P<0.05$, **$P<0.01$ (one-way ANOVA followed by Bonferroni's post-hoc test). (F) A representative image of the subcellular distribution of Raichu-Rab7 and mRFP–Rab7 in COS-7 cells. White lines indicate cell contours. Scale bar: 20 μm.

According to the design of this sensor, an increase in Rab7-GTP results in an increase in FRET, which can be represented by the ratio between 525 nm and 475 nm emission (Fig. 1C). Compared with the wild-type Rab7 sensor (green line), Raichu-Rab7-T22N, which has a reduced affinity to guanine nucleotides, exhibited a decreased ratio of FRET fluorescence intensity to CFP fluorescence intensity (FRET/CFP ratio) as expected (blue line). The FRET/CFP ratio of Raichu-Rab7-Q67L (red line), which lacks GTPase activity, was comparable to that of the wild-type Rab7 sensor, although the GTP loading of Raichu-Rab7-Q67L was 16.9% higher than that of Raichu-Rab7. We believe that the lack of an increase in the FRET/CFP ratio of Raichu-Rab7-Q67L, compared with Raichu-Rab7, might be the result of a small, but influential, conformational change in the Q67L mutant. Fig. 1D,E demonstrates that Raichu-Rab7 is capable of monitoring the balance between GEF and GTPase-activating protein (GAP) activities towards Rab7. In Fig. 1D, the expression of the GAP domain of Armus (Armus-GAP; Armus is also known as TBC1D2A) (Frasa et al., 2010) decreased the FRET/CFP ratio in a dose-dependent manner. The expression of both Mon1a and Ccz1 with Armus-GAP (Fig. 1E, column 3) increased the FRET/CFP ratio compared with cells expressing Armus-GAP only (column 2).

Next, we examined the subcellular distribution of Raichu-Rab7. Rab7 is associated with vesicular structures corresponding to late endosomes and lysosomes and distributed throughout the cytoplasm (Fig. 1F). The Rab7 sensor co-localised with authentic Rab7 in COS-7 cells (Fig. 1F). Furthermore, Raichu-Rab7 bound to RabGDI as efficiently as authentic Rab7 (S.Y. and T. Nakamura, unpublished data), suggesting that Raichu-Rab7 is also regulated by RabGDI.

Significant variation in Rab7 activity on individual endosomes in steady-state COS-7 cells

We first examined the spatial distribution of Rab7 activity in steady-state COS-7 cells in serum-free conditions. Raichu-Rab7 was localised to endosomes and was also present throughout the cytoplasm (Fig. 2Ab). In the cytoplasm Raichu-Rab7 is thought to bind RabGDI, which could distort the sensor conformation and energy transfer. Thus, in our study, we focused only on Rab7 activity on endosomes. To minimise any adverse effects of cytoplasmic sensors on the FRET/CFP ratio of endosomal sensors, we optimised the experimental conditions of confocal FRET imaging (see Materials and Methods). This method revealed that Rab7 on individual endosomes showed various levels of activity (Fig. 2Ac,d). Fig. 2B shows a histogram of the distribution of FRET/CFP ratios of Raichu-Rab7, Raichu-Rab7-Q67L and Raichu-Rab7-T22N on endosomes. Because the GTP loading of Raichu-Rab7-T22N was almost zero (Fig. 1B), the variation of its FRET/CFP ratio should theoretically be close to zero. Therefore, we consider that the observed deviation in the ratios of individual endosomes containing Raichu-Rab7-T22N (blue bars) from the average is caused by an intrinsic fluctuation partially associated with limitations in the present technique. We compared the distribution in the ratios of Raichu-Rab7 (1.59±0.16, mean±s.e.m.) and Raichu-Rab7-T22N (1.43±0.10) (Fig. S1A,B). The F-test revealed that the difference of these ratio distributions was statistically significant ($P<0.001$), demonstrating the presence of a significant net variation in Rab7 activity on different endosomes in steady-state COS-7 cells. The FRET/CFP ratio of Raichu-Rab7-Q67L also exceeded the fluctuation that the T22N mutant showed. This is consistent with the
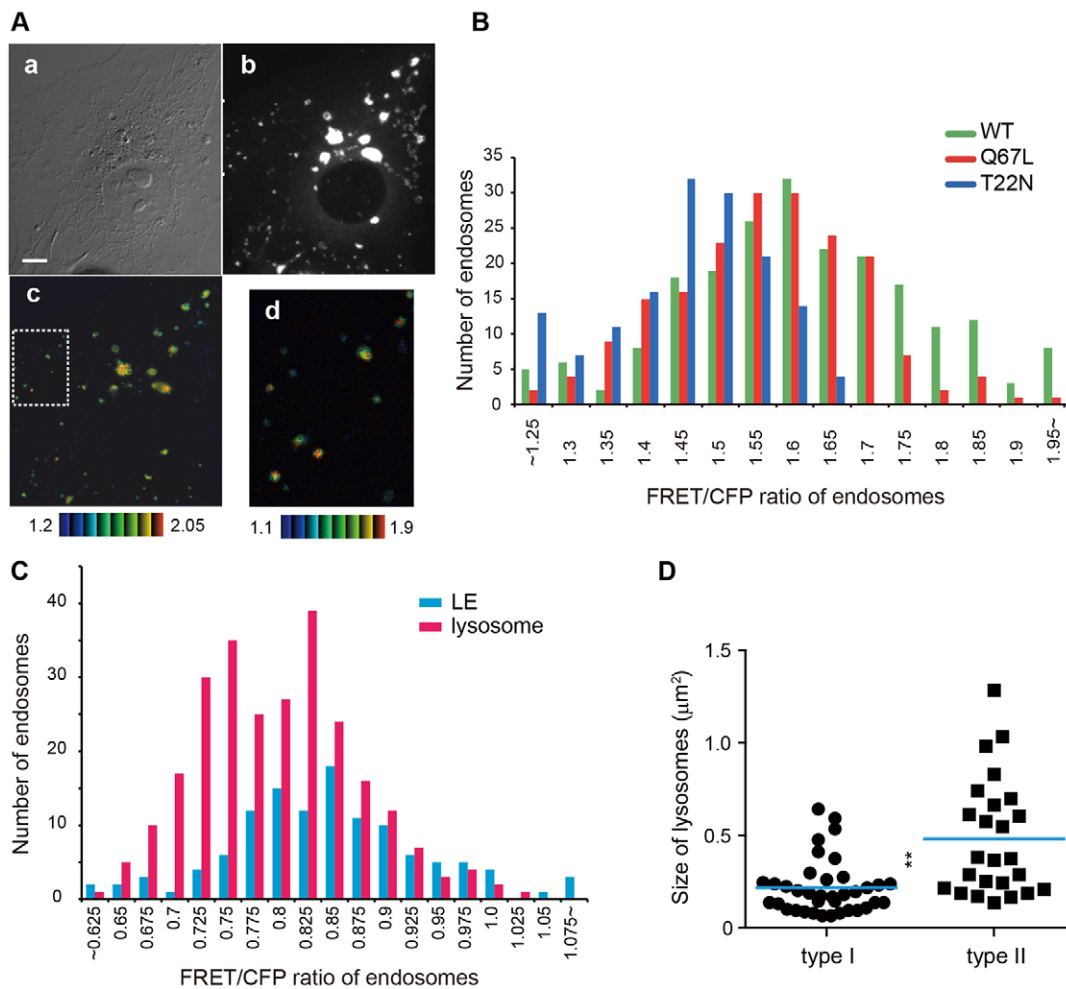
Fig. 2. Distribution of Rab7 activity in steady-state COS-7 cells. (A,B) COS-7 cells expressing Raichu-Rab7 sensors were observed by confocal microscopy for FRET imaging. (A) Representative images of the FRET/CFP ratio (c,d) of cells expressing a Raichu wild-type Rab7 sensor are shown cells are shown in an intensity-modulated display (IMD) mode, with corresponding DIC (a) and CFP (b) images. In the IMD mode, eight colours from red to blue are used to represent the FRET/CFP ratio, with the intensity of each colour indicating the mean intensity of FRET and CFP. The upper and lower limits of the ratio images are shown on the bottom. b shows a summation of sliced CFP images from the cell top to the cell bottom. c shows an image of the ratio of a summation of FRET intensity of three serial slices to that of CFP intensity of corresponding serial slices. d shows the enlarged ratio image corresponding to the boxed region in the panel c. Scale bar: 5 μm. (B) Distribution of FRET/CFP ratios of Raichu-Rab7 wild-type (WT, green), Raichu-Rab7-Q67L (red) and Raichu-Rab7-T22N (blue) on endosomes. Data from at least seven cells are shown in the histogram. (C) The A441-4 cell line was stained with Lyso-ID Red and examined using confocal FRET imaging. Blue and red bars correspond to late endosomes and lysosomes, respectively. Data from 15 cells are shown in the histogram. (D) A scatter plot depicts the size of endosomes in type I (lower FRET/CFP ratio) or type II (higher FRET/CFP ratio) lysosomes. Blue bars indicate the mean values: type I (*n*=37), type II (*n*=25). **P<0.01 (Student's *t*-test analysis).

fact that the GTP loading of Raichu-Rab7-Q67L was 54.0% (Fig. 2B), and thus the Q67L mutant also diverges from the average value. We similarly analysed the distribution of Rab7 activity on endosomes in HeLa cells (Fig. S1C), and found similar results.

The distribution of Rab7 activity on lysosomes exhibited two peaks in steady-state cells

We investigated the difference in Rab7 activity between late endosomes and lysosomes using a cell line derived from COS-7 cells, A441-4, which stably expresses Raichu-Rab7. These cells were stained with Lyso-ID Red and examined by confocal FRET imaging. Lyso-ID Red was less affected by photobleaching and exhibited more homogeneous staining than LysoTracker Red. Raichu-Rab7⁺ LysoID⁻ and Raichu-Rab7⁺ LysoID⁺ endosomes were classified as late endosomes and lysosomes, respectively. Fig. 2C shows the distribution of Rab7 activity on lysosomes (red

bars), which had two peaks. The distribution of lysosomal Rab7 activity was similar to a mixed normal distribution model, comprising two normal distributions, according to Akaike's information criterion (Akaike, 1973). This revealed that the lysosomes consisted of two populations, with distinct levels of Rab7 activity. It is known that lysosomes can be distinguished from endosomes by the lack of mannose-6-phosphate receptors [here, the cation-independent MPR (CI-MPR; encoded by *IGFR2*) has been studied]. (Luzio et al., 2007). Thus, we transfected an A441-4 cell line with pCIpre-mCherry-CIMPR-full and similarly analysed the cells. Raichu-Rab7⁺ CI-MPR⁺ and Raichu-Rab7⁺ CI-MPR⁻ endosomes were classified as late endosomes and lysosomes, respectively. In Fig. S1D, we can see that the distribution of Rab7 activity on lysosomes (without CI-MPR) also had two peaks. To reveal the identity of these two populations of lysosomes, we examined the size and distance from the nucleus of individual lysosomes, whose activities were close to the respective two peaks.

Lysosomes with higher Rab7 activity (type II) tended to be larger (0.48 ± 0.06 μm^2) than those having lower Rab7 activity (type I; 0.22 ± 0.02 μm^2, mean±s.e.m.) (Fig. 2D). There was no significant difference in the distance from the nucleus between the two lysosomal populations (Fig. S1E). Rab7 activity on late endosomes that were Lyso-ID Red-negative (Fig. 2C) or CI-MPR-positive (Fig. S1E) showed a single-peak distribution. The peak in the distribution of the FRET/CFP ratio on late endosomes was similar to the higher peak of lysosomes.

Increase in Rab7 activity on maturing macropinosomes in EGF-stimulated COS-7 cells

To investigate the change of Rab7 activity in the course of conversion from a single late endosome into a corresponding lysosome, we performed a time-lapse FRET imaging on maturing macropinosomes in epidermal growth factor (EGF)-stimulated COS-7 cells expressing Raichu-Rab7 and mCherry–CI-MPR (Fig. 3A,C). Macropinosomes, whose size ranges from 0.2 to 5.0 μm or more in diameter (Swanson, 2008), migrate in a centripetal manner and rapidly acquire late endosome markers, such as Rab7, before ultimately fusing with lysosomes (Movie 1; Racoosin and Swanson, 1993). Their large dimensions provide the means to readily analyse the change in endosomal Rab7 activity. The progress of macropinocytosis can be monitored using phase-contrast images in which the closure into discrete intracellular vesicles (cup closure) is characterised by a transition from phase-dark to phase-bright (Diakonova et al., 2002). Fig. 3A,C and Movie 2 show that the Rab7 sensor started to accumulate at macropinosomes around the timing of cup closure. During the following 10–25 min, Rab7 activity was at an intermediate level. Thereafter, Rab7 activity gradually increased for 20–40 min after cup closure until it reached its maximal level. CI-MPR appeared on macropinosomes around the timing of cup closure, and was removed on average 15–30 min afterwards. This disappearance of CI-MPR likely reflects the heterotypic fusion of macropinosomes with lysosomes. It is noteworthy that a further increase in Rab7 activity on macropinosomes (20–40 min after cup closure) paralleled the
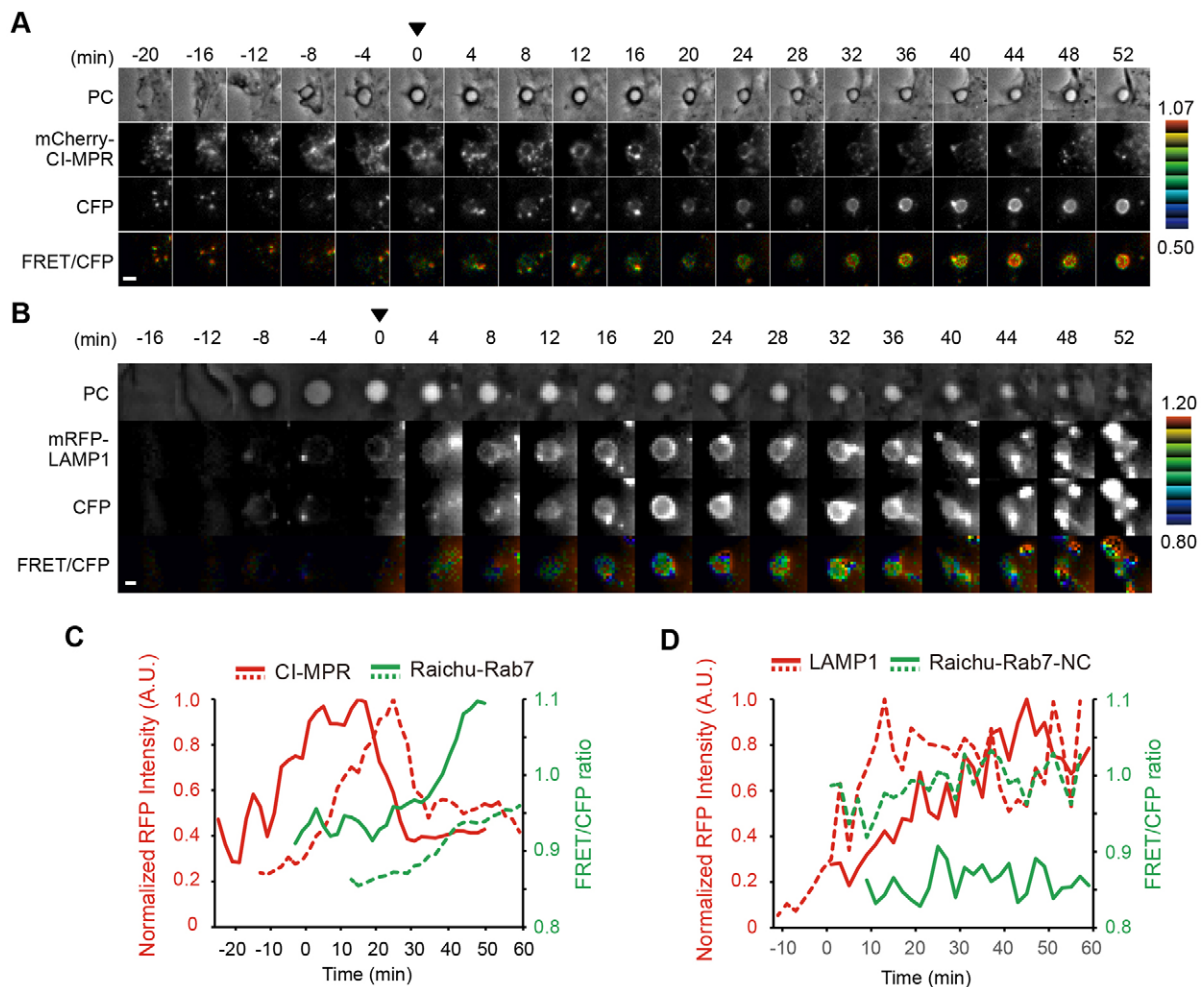

Fig. 3. Activation of Rab7 on endosomes during EGF-induced macropinocytosis. (A,C) COS-7 cells expressing Raichu-Rab7 and mCherry–CI-MPR were serum starved for 1 h and then stimulated with 50 ng/ml EGF. Images were obtained every 2 min for 2 h after stimulation. In A, representative ratio images of FRET/CFP of macropinosomes at the indicated time point (min) are shown in the IMD mode with the corresponding phase contrast (PC), mCherry and CFP images. The zero time point was set to be the frame corresponding to cup closure of a macropinosome (marked by a filled triangle). A corresponding movie of this macropinocytic event is shown in Movie 2. In C, two representative time-dependent changes in mCherry intensity (red lines) and the FRET/CFP ratio (green lines) are shown. Individual macropinocytic events are distinguishable by full or dotted lines. (B,D) COS-7 cells expressing Raichu-Rab7-NC and mRFP–LAMP1 were serum starved for 1 h and then stimulated with EGF. Images were obtained and shown as in A and C. Scale bars: 3 μm. A.U., arbitrary units.

decrease in mCherry–CI-MPR (15–30 min after cup closure) (Fig. S2A). We examined the specificity of the increase in Rab7 activity on maturing macropinosomes by a similar time-lapse experiment using Raichu-Rab7-NC as a negative control sensor, because the dominant-negative form, Racihu-Rab7-T22N, inhibits macropinosome formation and thus cannot be used. In Raichu-Rab7-NC, the Rab7-binding domain of Rabring7 was replaced with the Rab11-binding domain of GRAB (also known as RAB3IL1) (Horgan et al., 2013). Validation of this negative control was shown by the fact that the expression of Armus-GAP did not decrease the FRET/CFP ratio of Racihu-Rab7-NC (Fig. S2B). When Raichu-Rab7-NC was used in this experiment, the FRET/CFP ratio did not change during macropinocytosis (Fig. 3B,D; Fig. S2C,D). As shown in Fig. 3A, the level of Raichu-Rab7 on the early endosome state of macropinosomes was low, and thus we cannot obtain a reliable ratio image of Raichu-Rab7 there due to this technical limitation. To acquire information about the Rab7 activity on the early endosome state of macropinosomes, we examined the recruitment of EGFP–Mon1 to macropinosomes in COS-7 cells expressing RFP–APPL1, one of Rab5 effectors (Erdmann et al., 2007). As shown in Fig. S2E,F, the Mon1 level began to increase behind the rise in the level of APPL1 and reached a plateau at around the timing of the Rab5-to-Rab7 switch, roughly corresponding to cup closure (S.M. and T. Nakamura, unpublished data). Therefore, we presume that a large fraction of Rab7 on the early endosome state of macropinosomes is in a GDP-bound inactive state.

Rab7 depletion halts the transition of macropinosomes from late endosomes to lysosomes in EGF-stimulated COS-7 cells

During macropinosome maturation, Rab7 activity on late endosomes was not as high as on lysosomes (Fig. 3); thus, we examined the role of active Rab7 in late endosomes using an RNA interference (RNAi) approach. In COS-7 cells transfected with small interfering RNA (siRNA) against Rab7 (siRab7), 80% of endogenous Rab7 was depleted (Fig. S3A). COS-7 cells were transfected with control siRNA (siControl) or siRab7. The following day, the cells were further transfected with pCIpre-mCherry-CIMPR-full. After 24 h incubation, images were obtained every 2 min for 2 h after EGF stimulation. During stimulation, recombinant Clover fluorescent protein was simultaneously added to the medium as a cargo to monitor the progress of maturation. In siControl-transfected cells, Clover fluorescent protein had already been incorporated into macropinosomes at cup closure (Fig. 4A). Clover fluorescence disappeared abruptly within several minutes after cup closure (Fig. 4A,C). A decrease in mCherry–CI-MPR intensity on macropinosomes began at or just after cup closure. It is known that the pH of the late endosomes and lysosome are 5–6 and around 4.5, respectively (Huotari and Helenius, 2011; Saftig and Klumperman, 2009). Because the pKa of Clover is 6.2, the extinction of Clover fluorescence might begin on mature late endosomes. The decrease in mCherry–CI-MPR intensity showed that the late-endosome-to-lysosome transition of macropinosomes occurred at between 10 and 25 min after cup closure. Thus, dim Clover proteins might start to be degraded at ~15 min after cup closure. In Fig. S3B,D, we confirmed the timing of the transition of macropinosomes in control cells using LysoTracker Red. In contrast, in Rab7-depleted cells, the fluorescent intensity of Clover in macropinosomes did not change for more than 1 h after cup closure (Fig. 4B,D). The difference in fluorescent intensity

between control and Rab7-depleted cells was statistically significant (Fig. 4E). In Rab7-knockdown cells, the fluorescent intensity of mCherry–CI-MPR in macropinosomes increased around cup closure, similar to control cells, indicating that Rab7 depletion did not disturb the early-to-late endosomal transition of macropinosomes. A complementary experiment using LysoTracker Red (Fig. S3C,E) showed that macropinosomes containing Clover proteins did not transit to a lysosomal state in Rab7-depleted cells. Taken together, these results indicate that Rab7 depletion arrested macropinosome maturation on late endosomes and halted their transition into lysosomes.

Both Mon1 and Ccz1 are recruited to the late-endosomal state of macropinosomes and subsequently dissociate prior to fusion with lysosome

Next, we investigated the dynamics of Mon1 and Ccz1 recruitment on macropinosomes. The Mon1–Ccz1 complex has been shown to act as the main Rab7-specific GEF in mammalian cells (Gerondopoulos et al., 2012). During the fluid-phase uptake in *Caenorhabditis elegans* coelomocytes, Rab7 and SAND-1, the *C. elegans* ortholog of Mon1, are recruited simultaneously on endosomes. However, whereas SAND-1 persists on endosomes only for 2–3 min, Rab7 levels continue to rise (Poteryaev et al., 2010). In our study, we examined COS-7 cells expressing EGFP–Mon1a or EGFP–Ccz1 in combination with mCherry–CI-MPR to compare the behaviour of Mon1a or Ccz1 during the late-endosome-to-lysosome transition of macropinosomes. Mon1a and Ccz1 were recruited to macropinosomes shortly before cup closure, where they persisted for 10–15 min, and subsequently dissociated from macropinosomes, similar to CI-MPR (Fig. 5A–D). We further confirmed the timing of Mon1 detachment from macropinosomes using LysoTracker Red (Fig. S3F,G). These results indicate that Mon1–Ccz1 is recruited to the late-endosomal state of macropinosomes and dissociates from their lysosomal state in COS-7 cells.

COS-7 cells expressing EGFP–Mon1a were stained with Lyso-ID Red and the recruitment of Mon1a on lysosomes was examined. As shown in Fig. 5E, Mon1a-positive vesicles were distributed throughout cytoplasm, with very little overlap with lysosomes. Fig. 5F shows a correlation plot of EGFP–Mon1a and Lyso-ID Red intensities for individual endosomes. A group of endosomes with high EGFP signal (>3000) and relatively low LysoID signal were characterised as late endosomes. Endosomes exhibiting low Lyso-ID signal without EGFP–Mon1a were characterised as secretory vesicles, which are known to have a relatively low pH (Moreno et al., 2010). Then, we examined the overlap between EGFP–Mon1a and mCherry–CI-MPR in COS-7 cells (Fig. 5G). On average, 95% of Mon1a-positive endosomes contained CI-MPR (Fig. 5H). Taken together, these results indicate that Mon1a is mainly localised to late endosomes, but not to lysosomes, in COS-7 cells.

Although Mon1–Ccz1 is located only on late endosomes (Fig. 5), Figs 2 and 3 show that Rab7 is also active on lysosomes. Thus, we investigated the recruitment of Rab7 effectors during EGF-induced macropinocytosis. COS-7 cells expressing EGFP fusion proteins of one of seven Rab7 effectors and mCherry–CI-MPR were stimulated with EGF, and then imaged every 2 min. Vps41, a subunit of the HOPS complex, was recruited to the late-endosomal state of macropinosomes at almost the same time as CI-MPR, frequently persisted after the CI-MPR removal, and eventually dissociated several tens of minutes after recruitment (Fig. S4A,D). In contrast, RILP (SwissProt ID Q5ND29) (Fig. S4B,E) and PLEKHM1 (Fig. S4C,F) were recruited to the lysosomal state of
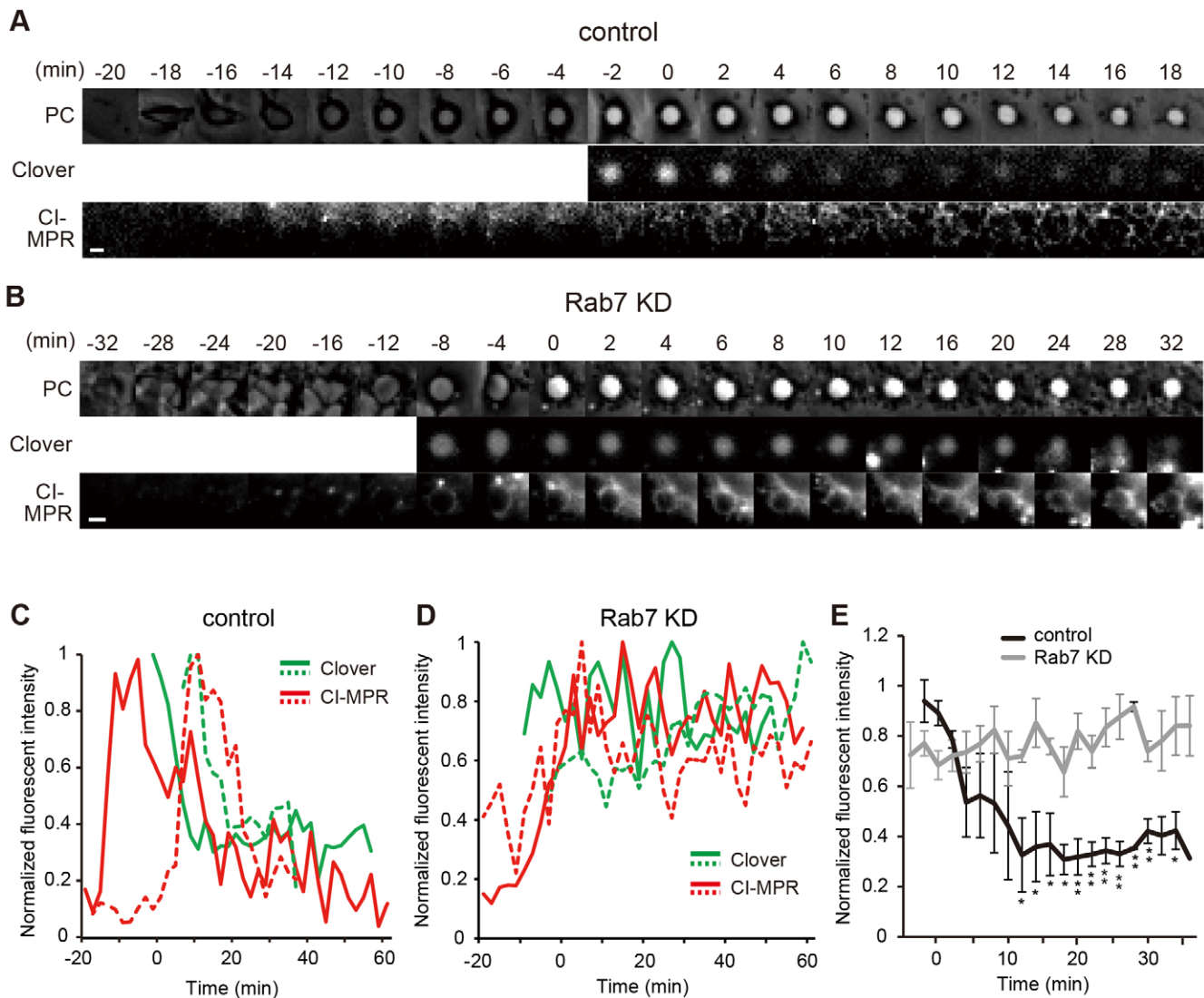
Fig. 4. Effect of Rab7 depletion on EGF-induced macropinocytosis. COS-7 cells were transfected with control (A,C) or Rab7 siRNA (KD) (B,D). After 24 h incubation, the cells were further transfected with pCIpre–mCherry-CIMPR-full. After serum starvation for 1 h, images were obtained every 2 min for 2 h after addition of EGF and 5 µg/ml of recombinant Clover. After pausing of the imaging at an appropriate time, the medium containing Clover was replaced by fresh imaging medium and imaging was resumed. The zero time point was set to be the frame corresponding to cup closure of a macropinosome. In A and B, representative phase contrast (PC), Clover and mCherry (CI-MPR) images of macropinosomes in the control (A) or Rab7-depleted (B) cells at the indicated time point (min) are shown. Scale bars: 3 µm. In C and D, two representative time-dependent changes in Clover intensity (green lines) and mCherry–CI-MPR intensity (red lines) of macropinosomes in the control (C) or Rab7-depleted (D) cells are shown. Individual macropinocytic events are distinguishable by full or dotted lines. (E) The mean±s.e.m. of normalised Clover intensity of macropinosomes at the indicated time-points in the control or Rab7-depleted cells are shown. The number of experiments was control (n=4) and Rab7-depleted (n=4). *P<0.05; **P<0.01 (Student's t-test).

macropinosomes in place of CI-MPR. The behaviour of RILP and PLEKHM1 supports the idea that active Rab7 plays roles on lysosome as well as on late endosomes.

Rab7 activation on lysosomes is independent of Mon1–Ccz1 in HeLa cells

The finding that lysosomes are devoid of Mon1–Ccz1 raises the possibility that Rab7 activity on lysosomes, shown in Figs 2 and 3, is independent of Mon1–Ccz1. To explore this possibility, we examined the effect of Ccz1 depletion on Rab7 activity on late endosomes and lysosomes. Because mammals have two Mon1 isoforms, it might be difficult to completely deplete both Mon1 proteins. As shown in Fig. 6A, Ccz1 siRNA (siCcz1) efficiently reduced the amount of endogenous Ccz1 in HeLa (85%

depletion) and COS-7 cells (80% depletion). One day after transfection with siControl or siCcz1, HeLa cells were transfected with Raichu-Rab7. After 24 h incubation, the cells were stained with Lyso-ID Red and examined by confocal FRET imaging. The distribution of Rab7 activity on late endosomes and lysosomes in siControl-transfected cells (Fig. 6B, left) was essentially the same as that shown in Fig. 2C. In Ccz1-depleted cells (Fig. 6B, right), the distribution of Rab7 activity on late endosomes (blue bars) shifted towards a lower level than that in control cells, as expected from the residence of Mon1–Ccz1 on late endosomes. The averages of the FRET/CFP ratios on late endosomes in control and Ccz1-depleted cells were 0.77±0.01 and 0.70±0.01 (mean±s.e.m.), respectively (Fig. 6C). This difference was statistically significant (P<0.01). In contrast,
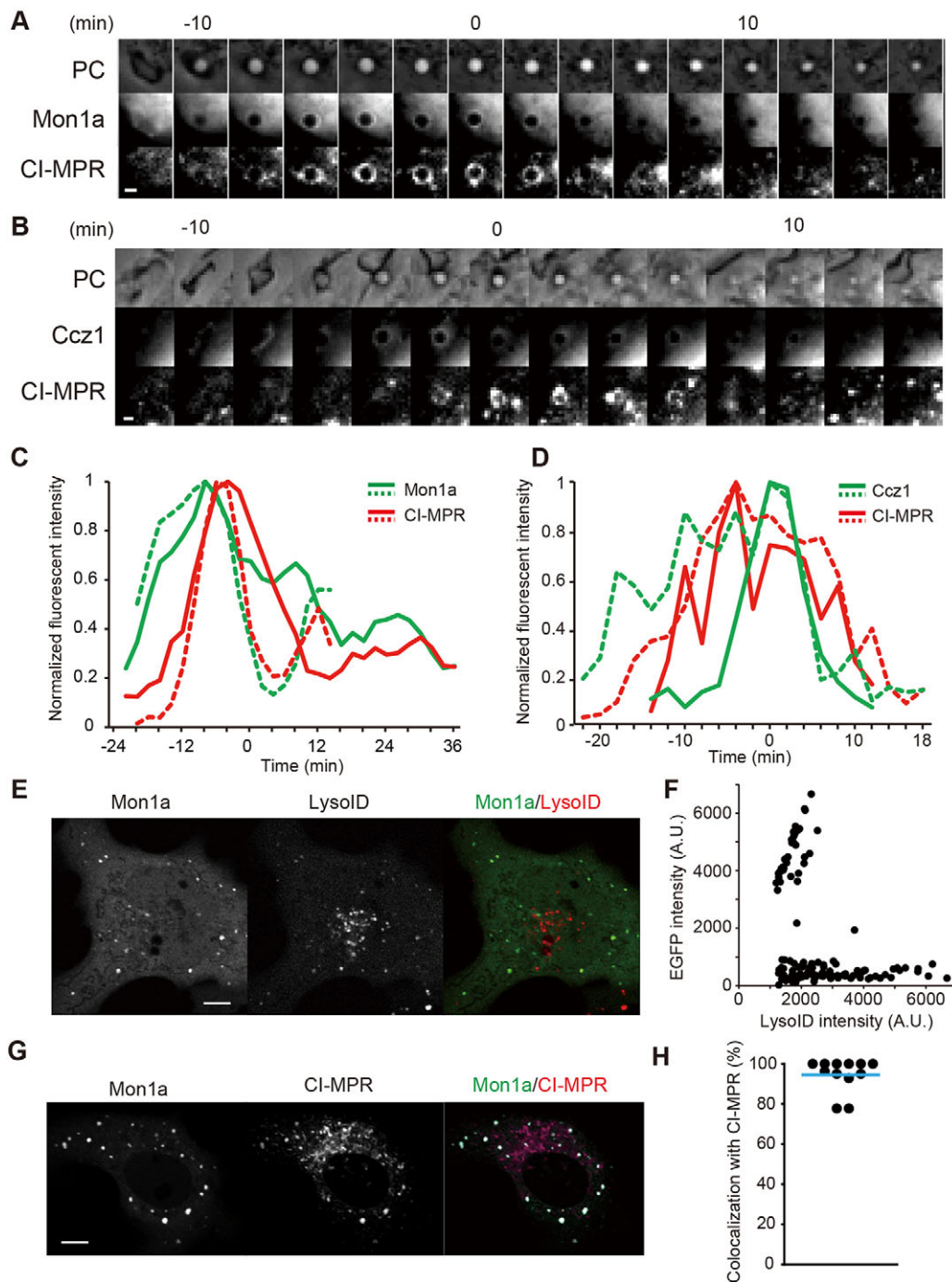
Fig. 5. Recruitment and detachment of Mon1–Ccz1 on EGF-induced macropinosomes in COS-7 cells. (A–D) COS-7 cells expressing EGFP–Mon1a (A,C) or EGFP–Ccz1 (B,D) in combination with mCherry–CI-MPR were starved for 1 h and then stimulated with EGF. Images were obtained every 2 min for 2 h after stimulation. In A and B, representative EGFP–Mon1a (A) and EGFP–Ccz1 (B) images of macropinosomes at the indicated time points (min) are shown with the corresponding phase contrast (PC) and mCherry-CI-MPR images. Scale bars: 3 µm. The zero time point was set to be the frame corresponding to cup closure of a macropinosome. In C and D, two representative time-dependent changes in EGFP (green lines) and mCherry (red lines) intensities are shown. Individual macropinocytic events are distinguishable by full or dotted lines. (E,F) COS-7 cells expressing EGFP–Mon1a were stained with Lyso-ID Red and observed using confocal microscopy. In E, representative images of the subcellular distribution of Mon1a (left) and lysosomes (centre) are shown with a merged image (right). Scale bar: 5 µm. In F, the fluorescent intensity of EGFP–Mon1a and Lyso-ID Red on individual endosomes was plotted. Data from five cells are shown in the plot. (G,H) COS-7 cells expressing EGFP–Mon1a and mCherry–CI-MPR were observed using confocal microscopy. In G, representative images of the subcellular distribution of Mon1a (left) and CI-MPR (centre) are shown with a merged image (right). Scale bar: 5 µm. In H, a scatter plot depicts the percentage of Mon1a-containing endosomes that also had CI-MPR in individual cells (*n*=12). The blue bar indicates the mean value.

there was no significant difference in the distribution of Rab7 activity on lysosomes between control (0.73±0.01) and Ccz1-depleted (0.74±0.01) cells (Fig. 6C). Taken together, the results

of confocal FRET imaging show that Rab7 activation on late endosomes, but not on lysosomes, is dependent on the Mon1–Ccz1 complex.
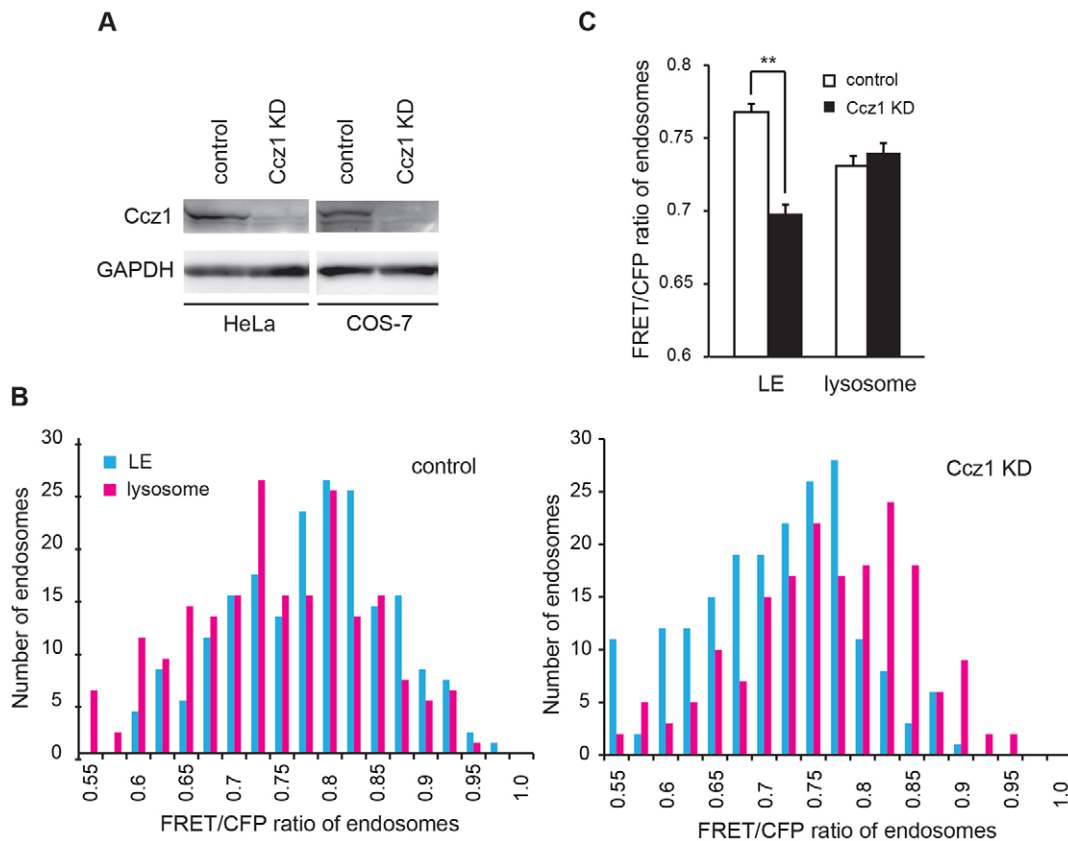
Fig. 6. Effect of Ccz1 depletion on Rab7 activity on late endosomes and lysosomes in steady-state HeLa cells. (A) HeLa or COS-7 cells were transfected with control or Ccz1 siRNA (KD). After incubation for 2 days, the cells were analysed by immunoblotting with anti-Ccz1 or anti-GAPDH antibodies. Experiments were repeated three times. (B,C) HeLa cells were transfected with control or Ccz1 siRNA. Thereafter, the cells were further transfected with pRaichu-Rab7. After incubation for 1 day, the cells were stained with Lyso-ID Red and observed by confocal microscopy for FRET imaging. Raichu-Rab7$^+$ LysoID$^-$ and Raichu-Rab7$^+$ LysoID$^+$ endosomes were classified as late endosomes (blue) and lysosomes (red), respectively. Data from 392 endosomes from 20 cells (control) or 377 endosomes from 20 cells (Ccz1 KD) are shown in the histograms. In C, a bar graph shows the mean±s.e.m. of the FRET/CFP ratios of late endosomes or lysosomes in control (white) or Ccz1-depleted (black) cells. **P<0.01 (one-way ANOVA followed by Bonferroni's post-hoc test).

Ccz1 depletion does not affect the active Rab7-dependent perinuclear accumulation of lysosomes in COS-7 cells

To confirm the independence of lysosomal Rab7 activity from Mon1–Ccz1, we examined the Rab7-dependent perinuclear accumulation of lysosomes in the presence or absence of Ccz1. It has been shown that expression of Rab7-T22N causes selective dispersal of perinuclear lysosomes without any noticeable effects on late endosomes (Bucci et al., 2000). In Fig. 7A,B, COS-7 cells were transfected with siControl or siRab7 and stained with Lyso-ID Red after incubation for 2 days. In control conditions, almost all cells (clustered, 49.8%; intermediate, 46.7%) showed the perinuclear accumulation of lysosomes. However, 70.1% of Rab7-depleted cells showed dispersion of lysosomes. This result indicates that the perinuclear accumulation of lysosomes requires Rab7. It is thought that perinuclear clustering of lysosomes is mediated by RILP, which binds to Rab7-GTP and the p150^{Glued} (also known as DCTN1) subunit of the dynein–dynactin complex, and is responsible for minus-end transport on microtubules (Johansson et al., 2007). Therefore, the result in Fig. 7A,B is consistent with the recruitment of RILP to lysosomes, which is shown in Fig. S4B,E. Next, we examined the effect of Ccz1 depletion on lysosome positioning. There was no significant difference in perinuclear lysosome accumulation between control and Ccz1-depleted cells (Fig. 7C,D). This result further supports the concept that Rab7 activation on lysosomes is independent of Mon1–Ccz1.

DISCUSSION

In this study, we demonstrated that, in mammalian cells, Rab7 activity on late endosomes, but not on lysosomes, depends on Mon1–Ccz1. This is supported by our findings that (1) Ccz1 depletion did not change Rab7 activity on lysosomes even though it resulted in a significant decrease in Rab7 activity on late endosomes (Fig. 6), and that (2) the perinuclear accumulation of lysosomes occurred irrespectively of the presence or absence of Ccz1, whereas they were dispersed throughout cells lacking Rab7 (Fig. 7). Consistent with this idea, Mon1 and Ccz1 were recruited to the late-endosomal state of macropinosomes and detached from their lysosomal state during macropinocytosis (Fig. 5). A similar dissociation of Mon1 shortly after its recruitment to endosomes has been previously reported in fluid-phase uptake in C. elegans coelomocytes (Poteryaev et al., 2010).

Mon1–Ccz1 is the only known Rab7 GEF, and its activity has been demonstrated in yeast and humans (Gerondopoulos et al., 2012; Nordmann et al., 2010). However, there has been much debate as to where Mon1–Ccz1 works with Rab7. In yeast, it has been suggested that Mon1–Ccz1 function is primarily confined to late endosomes, based on their localisation (Nordmann et al., 2010). However, other studies have reported that deletion of either Mon1 or Ccz1 leads to vacuole fragmentation (Wang et al., 2002) and that Mon1 is recruited to both endosomes and vacuoles by phosphatidylinositol 3-phosphate (PI3P) (Lawrence et al., 2014).
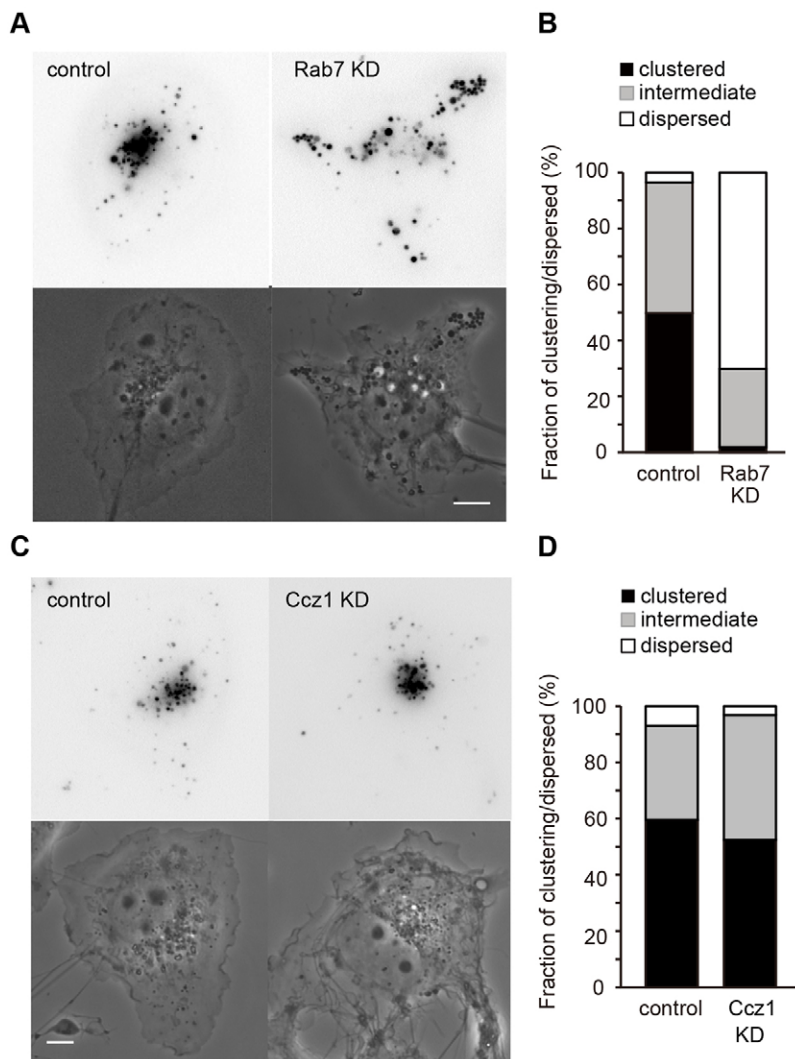
Fig. 7. Effect of Rab7 or Ccz1 depletion on the perinuclear accumulation of lysosomes in steady-state COS-7 cells. (A,B) COS-7 cells were transfected with control or Rab7 siRNA (KD). After incubation for 2 days, the cells were stained with Lyso-ID Red and then imaged. In A, representative images of the subcellular distribution of lysosomes in control (top left) or Rab7-depleted (top right) cells are shown with corresponding DIC images (bottom). The distribution of lysosomes was classified into three categories: clustered, almost all lysosomes were localised to the perinuclear area (e.g. top left); intermediate, some lysosomes existed in the cell periphery although a large number were localised to perinuclear area; or dispersed, lysosomes were distributed throughout the cell (e.g. top right). In B, a bar graph shows the percentage of cells in the three categories in control (left) or Rab7-depleted (right) cells. (C,D) COS-7 cells were transfected with control or Ccz1 siRNA. After incubation for 2 days, the cells were stained with Lyso-ID Red and then imaged. Representative images (C) of the subcellular distribution of lysosomes and the percentage of cells in the the three categories (D) in control or Rab7-depleted cells are shown as in A and B. Scale bars: 10 μm.

In *Drosophila*, loss of function of Mon1 resulted in an enlargement of maturing endosomes, but lysosome formation was unaffected (Yousefian et al., 2013). However, previous studies on Mon1–Ccz1 could not discriminate among presumed multiple Mon1–Ccz1 functions, such as its role in Rab7 activation as a GEF (Nordmann et al., 2010), in HOPS recruitment (Poteryaev et al., 2010) and in Rab7 recruitment to the endosomal membrane (Kinchen and Ravichandran, 2010). Therefore, we examined whether Mon1–Ccz1 is implicated in Rab7 activation either on late endosomes or lysosomes (or both) using a Rab7 sensor and found that, in mammals, Rab7 activity on late endosomes, but not on lysosomes, depends on Mon1–Ccz1. This means that the Mon1–Ccz1 complex activates Rab7 only on late endosomes. Our findings indicate that one or more additional and presently unknown Rab7 GEFs are responsible for Rab7 activation on lysosomes.

A major function of Rab7 in the endolysosomal pathway is mediating membrane fusion in coordination with the HOPS tethering complex, although there have been conflicting views about the exact role of Rab7 in membrane fusion between endosomes (Nordmann et al., 2012). Rab7 depletion and Rab7-T22N expression in EGF-treated HeLa cells strongly inhibit EGFR exit from late endosomes, and cause an accumulation of densely packed and enlarged late endosomes (Ceresa and Bahr, 2006; Vanlandingham and Ceresa, 2009). In the absence of Rab7,

lysosomes do not fuse with phagosomes containing apoptotic cells in *C. elegans* (Guo et al., 2010). These results indicate that Rab7 plays an essential role in the fusion between late endosomes and lysosomes, and is not required for movement of cargo from early endosomes to late endosomes. However, some groups have claimed that Rab7 is recruited to early endosomes and mediates sorting and transport of cargos to late endosomes depending on the type of cargo and/or sorting events (Girard et al., 2014; Vonderheit et al., 2005). The present study on macropinocytosis has shown that Rab7 depletion disturbed the transition from late endosomes to lysosomes, corroborating the opinion that Rab7 plays an essential role in the fusion between late endosomes and lysosomes. In EGF-induced macropinosomes, Rab7 activity was maintained at a relatively high level after endolysosomal formation. Therefore, active Rab7 should not only be implicated in the fusion of late endosomes with lysosomes, but also in other endosomal processes, such as intracellular localization of lysosomes (Fig. 7), lysosomal biogenesis (Bucci et al., 2000) and retromer recruitment to endosomal membranes (Rojas et al., 2008).

The finding that lysosomes in unstimulated COS-7 cells were separated into two populations with different Rab7 activity emphasises the heterogeneity of lysosomes (Huotari and Helenius, 2011). Fig. 2D shows that lysosomes with higher Rab7 activity tend to be larger in size than those with lower activity. Thus,

the population with higher Rab7 activity might have higher fusing capabilities, which allows them to continue to fuse with late endosomes and other lysosomes, resulting in larger vesicles. In general, the fusion of late endosomes with lysosomes generates a transient hybrid organelle, called an endolysosome, in which active degradation takes place (Bright et al., 1997; Mullock et al., 1998). This endolysosome might correspond to the population with higher Rab7 activity. The endolysosome is converted into a mature lysosome, which constitutes a storage organelle for lysosomal hydrolases and other degrading enzymes (Huotari and Helenius, 2011). The puncta with lower Rab7 activity in Fig. 2C might indeed correspond to mature lysosomes. Because lysosomes have been reported to have divergent functions, such as secretion, plasma membrane repair and energy metabolism in addition to their degradative function (Settembre et al., 2013), these organelles should be regarded as a heterogeneous population (Huotari and Helenius, 2011). What kind of functional divergence exits between lysosomal pools with different Rab7 activity is an attractive subject for future research.

The present study demonstrated that Rab7-GDP was localised on endosomal membranes, and, in EGF-stimulated COS-7 cells, Rab7 was initially recruited to macropinosomes in a GDP-bound inactive form and subsequently became activated during maturation, eventually leading to fusion with lysosomes. These results indicate that an unknown factor exists, which can deliver Rab7-GDP onto endosomal membranes. Rab GEFs display the minimal targeting machinery for targeting Rabs from the cytosol to the correct compartment (Blumer et al., 2013). For Rab1, *Legionella pneumophila* DrrA has remarkably efficient GEF activity, and its GEF activity is sufficient to displace the GDI from the Rab1–GDI complex (Schoebel et al., 2009). Rab GEFs vary tremendously in their catalytic efficiency, and the endpoint of the GDI displacement is determined by the relative affinities of Rab-GDP and Rab-GTP to the GDI and the ratio between the GTP and GDP concentration (Schoebel et al., 2009). The efficiency of Mon1–Ccz1 GEF activity is moderate ($2000\ \mathrm{M}^{-1}\ \mathrm{s}^{-1}$) and slower than DrrA and TRAPP (Cai et al., 2008; Nordmann et al., 2010; Schoebel et al., 2009). Thus, we believe that Mon1–Ccz1 cannot facilitate the displacement of GDI from Rab7-GDP, but that an unidentified GDF dissociates the Rab7–GDI complex for delivery of Rab7 to the endosomal membrane. For Rab9, the integral membrane protein Yip3 acts catalytically to dissociate complexes of Rab9 bound to GDI, and to deliver it onto membranes (Sivars et al., 2003). Lgl1 interacts directly with Rab10-GDP and acts to release GDI from Rab10 (Wang et al., 2011). Future studies aiming at the identification of novel GDFs acting on Rab7 are essential for uncovering the mechanism controlling the localisation and activity of Rab7 in the endolysosomal network.

MATERIALS AND METHODS
FRET biosensors
pRaichu-Rab7/A441, derived from the pCAGGS expression vector, encoded a FRET biosensor based on the Eevee backbone (a gift from Michiyuki Matsuda, Kyoto University, Japan; Komatsu et al., 2011), designated Raichu-Rab7, which comprised YPet-GL (Nguyen and Daugherty, 2005), the Rab7-binding domain of mouse Rabring7 (amino acids 10–145; Mizuno et al., 2003), SECFP (a brighter version of CFP developed by Atsushi Miyawaki, RIKEN Brain Research Institute, Japan), and canine Rab7 (a gift from Yoshimi Takai, Kobe University, Japan). The flexible linkers, collectively designated MeV (modified evading), consisted of the 15-amino-acid peptide (GGSGG)$_3$, between YPet-GL and the Rab7-binding domain of Rabring7, the EV linker of 116 amino acids (Komatsu et al., 2011) between the RBD domain of Rabring7 and

SECFP, and the 15-amino-acid peptide, (GGSGG)$_3$, between SECFP and Rab7. If necessary, wild-type Rab7 was replaced with Rab7-Q67L or Rab7-T22N. In pRaichu-Rab7-NC, the Rab7-binding domain of Rabring7 was replaced with the Rab11-binding domain of GRAB (Horgan et al., 2013).

Plasmids
The cDNAs for wild-type Rab7, Rab7-Q67L and Rab7-T22N were subcloned into pCAGGS-EGFP and pCXN2-mRFP (Ohba et al., 2003). The cDNA for a GAP domain of Armus (a gift from Vania M. Braga, Imperial College, London, UK; Frasa et al., 2010) was subcloned into the pCAGGS expression vector. The cDNAs for mouse Mon1a and Ccz1 were obtained by conventional PCR techniques (Fukuda et al., 1999) and subcloned into pEGFP-C1 (Clontech, Mountain View, CA). The RILP cDNA was subcloned into pCAGGS-EGFP. pEGFP-C1-PLEKHM1 (Tabata et al., 2010) and pmRFP-N1-Lamp1 (Kimura et al., 2007) were provided by Tamotsu Yoshimori (Osaka University, Japan). pcDNA3-RFP-APPL1 (Erdmann et al., 2007) was provided by Pietro De Camilli (Yale University, New Haven, CT). The cDNA for CI-MPR (CI-MPR is also known as IGF2R) (Waguri et al., 2006) was used to prepare pCIpre-mCherry-CIMPR-full. The cDNA for mouse Vps41 was amplified by PCR and subcloned into pmStr-C1 (Ohbayashi et al., 2012). The piggyBac transposon-based expression vector (Yusa et al., 2009) was provided by Allan Bradley (Wellcome Trust Sanger Institute, UK).

Cells, reagents and antibodies
293-F cells (Life Technologies, Carlsbad, CA) were maintained in FreeStyle 293 expression medium (Life Technologies). COS-7 and HeLa cells were maintained in Dulbecco's modified Eagle's medium (DMEM) containing 10% fetal bovine serum. A cell line derived from COS-7 cells, A441-4, which stably expresses Raichu-Rab7, was established as described previously (Yusa et al., 2009). EGF was purchased from Calbiochem (La Jolla, CA). Lyso-ID Red was obtained from Enzo Life Sciences (Farmingdale, NY). The following primary antibodies were used: rabbit polyclonal antibodies to Rab7 (1:300 dilution, R4779, Sigma-Aldrich, St Louis, MO); goat polyclonal antibodies to Ccz1 (1:500 dilution, T-19, Santa Cruz Biotechnology, Santa Cruz, CA); and rabbit polyclonal antibodies to GAPDH (1:1000 dilution, FL-335, Santa Cruz Biotechnology). Anti-GFP polyclonal antibody was a gift from Naoki Mochizuki (NCVC Research Institute, Japan), and 2 µl of antibody was used for immunoprecipitation.

RNA interference
Rab7 Stealth siRNA and Ccz1 Silencer Select siRNA were obtained from Life Technologies. The 25mer nucleotide sequence (sense) to target human and monkey Rab7 mRNA was 5′-CAUUCAUGAACCAGUAUGUGAA-UAA-3′. The nucleotide sequence (sense) to target human and monkey Ccz1 mRNA was 5′-GCUCAUCUGGAGUGGAUUAGAACAA-3′. COS-7 or HeLa cells were transfected with 20 nM siRNA using Lipofectamine RNAiMAX (Life Technologies) according to the manufacturer's instructions and used after 48 h incubation.

In vitro spectrofluorometry
At 48 h after transfection, 293-F cells were transferred into a quartz cuvette and fluorescence spectra were obtained using an FP-750 spectrometer (JASCO, Hachioji, Japan) at an excitation wavelength of 433 nm.

Analysis of guanine nucleotides bound to Rab7
Guanine nucleotides bound to Raichu sensors or EGFP–Rab7 were analysed as previously described (Kawase et al., 2006). Briefly, COS-7 cells were transfected with pRaichu-Rab7 or pCAGGS-EGFP-Rab7. At 36 h after transfection, cells were labelled with ^{32}P$_i$ in phosphate-free modified Eagle's medium (Life Technologies) for 4 h. Raichu-Rab7 and EGFP–Rab7 were immunoprecipitated with anti-GFP antibodies. The immunoprecipitates were analysed by thin layer chromatography. GTP and GDP bound to Rab7 were quantified using a FLA-7000 image analyser (Fuji Film, Tokyo, Japan).

Time-lapse FRET imaging

COS-7 cells expressing FRET sensors were serum-starved for 1 h with FluoroBrite DMEM medium (Life Technologies) containing 0.1% BSA and 4 mM L-glutamine prior to stimulation with 50 ng/ml EGF. The medium was covered with mineral oil (Sigma-Aldrich) to prevent evaporation. Cells were imaged at 37°C with an IX81 inverted microscope (Olympus, Tokyo, Japan) equipped with a Cool SNAP-HQ cooled charge-coupled device camera (Roper Scientific, Trenton, NJ), a laser auto-focusing system (IX2-ZDC, Olympus) and an automatically programmable XY stage (MD-XY30100T-Meta, SIGMA KOKI, Tokyo, Japan), which allowed time-lapse images of several fields of view to be obtained in a single experiment. The following filters were used for dual-emission imaging: an FF01-438/24-25 excitation filter (Semrock, Rochester, NY); an XF2034 (455DRLP) dichroic mirror (Omega Optical, Brattleboro, VT); and two emission filters (FF01-483/32-25 for CFP and FF01-542/27-25 for FRET, Semrock). Cells were illuminated with a 75-W Xenon lamp through a 6% neutral density filter or an X-Cite 120LED (Lumen Dynamics, Mississauga, Canada), and viewed through a Plan Apochromat 60× oil objective lens (NA 1.4, Olympus). The exposure times for 4×4 binning were 200 ms for CFP and FRET images and 100 ms for phase contrast images. After background subtraction, FRET/CFP ratio images were created with MetaMorph software (Universal Imaging, West Chester, PA), and the images were used to represent FRET efficiency according to Kawase et al. (2006) with some modifications. Single macropinocytic events were selected manually, and the macropinosome was centred in the image. The local background was determined as the average fluorescence of the region surrounding the target macropinosome, with a three-pixel width, corresponding to 0.225 μm.

Confocal microscopy

Cells were fixed with 3.7% formaldehyde. After washing with PBS, the samples were imaged with an IX81 inverted microscope equipped with an FV-1000 confocal imaging system (Olympus) using a Plan Apochromat 60× oil objective lens (NA 1.4, Olympus).

For confocal FRET imaging, HeLa or COS-7 cells expressing FRET sensors were cultured with FluoroBrite DMEM medium containing 0.1% BSA and 4 mM L-glutamine and then imaged with the IX81 inverted microscope equipped with the FV-1000 confocal imaging system and a PlanApoN 60× oil objective lens (NA 1.4, Olympus) at 37°C. The excitation laser and fluorescence filter settings were as follows: excitation laser, 440 nm; excitation dichroic mirror, DM405–440; CFP channel PMT dichroic mirror, SDM 510; CFP channel PMT filter, BA460–490; FRET channel PMT filter, BA515–615. For Lyso-ID-Red-stained cells, the wavelength of the excitation laser was 559 nm and the filter settings for red fluorescence were as follows: excitation dichroic mirror, BS20/80; RFP channel PMT filter, BA575–675. For Rab7 sensors, images were obtained in a fixed condition (laser power 2%; scan speed 20 μs/pixel; confocal aperture, 100 μm; slice width, 0.42 μm; 2× zoom). Image processing was performed with MetaMorph software. A summation image of three serial planes where the endosomes were clearly visible was created and subjected to background subtraction. Using Top-hat morphological filtering, individual endosomes, whose areas were 10–500 pixels and fluorescent intensities in CFP and FRET channels were ≥500, were selected. Endosomes with aberrant morphologies were eliminated by sight. Thereafter, CFP and FRET fluorescent intensities were obtained for individual endosomes and FRET/CFP ratios were calculated. If necessary, RFP intensities from Lyso-ID Red were similarly obtained. According to their red fluorescent intensities, endosomes were classified as late endosomes (<1000) or lysosomes (≥1000).

Preparation of recombinant Clover protein

Clover (a gift from Michael Lin, Stanford University, CA; Lam et al., 2012) was produced using the pGEX-6P expression vector (GE Healthcare, Little Chalfont, UK). GST–Clover proteins were purified using glutathione–Sepharose and cleaved with Precision protease (GE Healthcare). The purity of the eluted Clover was checked by SDS-PAGE.

Statistical analysis

One-way ANOVA followed by Dunnett's or Bonferroni's post-hoc tests were performed using GraphPad PRISM (version 5.04, GraphPad Software, San Diego, CA). Evaluation of the fitting of the distribution of Rab7 activity on lysosomes with a mixed normal distribution according to Akaike's information criterion (Akaike, 1973; Burnham and Anderson, 1998) was implemented by MATLAB software (2015a, MathWorks, Natick, MA).

Supplementary information
Supplementary information available online at
http://jcs.biologists.org/lookup/suppl/doi:10.1242/jcs.178095/-/DC1

References
Akaike, H. (1973). Information theory and an extension of the maximum likelihood principle. In *Proceedings of the 2nd International Symposium* (ed. B. N. Petrov and F. Csáki), pp. 267-281. Budapest: Akadémiai Kiado.

Blumer, J., Rey, J., Dehmelt, L., Mazel, T., Wu, Y.-W., Bastiaens, P., Goody, R. S. and Itzen, A. (2013). RabGEFs are a major determinant for specific Rab membrane targeting. *J. Cell Biol.* **200**, 287-300.

Bright, N. A., Reaves, B. J., Mullock, B. M. and Luzio, J. P. (1997). Dense core lysosomes can fuse with late endosomes and are re-formed from the resultant hybrid organelles. *J. Cell Sci.* **110**, 2027-2040.

Bucci, C., Thomsen, P., Nicoziani, P., McCarthy, J. and van Deurs, B. (2000). Rab7: a key to lysosome biogenesis. *Mol. Biol. Cell* **11**, 467-480.

Burnham, K. P. and Anderson, D. R. (1998). *Model Selection and Inference: A Practical Information-Theoretical Approach.* New York: Springer-Verlag.

Cai, Y., Chin, H. F., Lazarova, D., Menon, S., Fu, C., Cai, H., Sclafani, A., Rodgers, D. W., De La Cruz, E. M., Ferro-Novick, S. et al. (2008). The structural basis for activation of the Rab Ypt1p by the TRAPP membrane-tethering complexes. *Cell* **133**, 1202-1213.

Ceresa, B. P. and Bahr, S. J. (2006). rab7 activity affects epidermal growth factor: epidermal growth factor receptor degradation by regulating endocytic trafficking from the late endosome. *J. Biol. Chem.* **281**, 1099-1106.

Diakonova, M., Bokoch, G. and Swanson, J. A. (2002). Dynamics of cytoskeletal proteins during Fcγ receptor-mediated phagocytosis in macrophages. *Mol. Biol. Cell* **13**, 402-411.

Erdmann, K. S., Mao, Y., McCrea, H. J., Zoncu, R., Lee, S., Paradise, S., Modregger, J., Biemesderfer, D., Toomre, D. and De Camilli, P. (2007). A role of the Lowe syndrome protein OCRL in early steps of the endocytic pathway. *Dev. Cell* **13**, 377-390.

Frasa, M. A. M., Maximiano, F. C., Smolarczyk, K., Francis, R. E., Betson, M. E., Lozano, E., Goldenring, J., Seabra, M. C., Rak, A., Ahmadian, M. R. et al. (2010). Armus is a Rac1 effector that inactivates Rab7 and regulates E-cadherin degradation. *Curr. Biol.* **20**, 198-208.

Fukuda, M., Kanno, E. and Mikoshiba, K. (1999). Conserved N-terminal cysteine motif is essential for homo- and heterodimer formation of synaptotagmins III, V, VI, and X. *J. Biol. Chem.* **274**, 31421-31427.

Gerondopoulos, A., Langemeyer, L., Liang, J.-R., Linford, A. and Barr, F. A. (2012). BLOC-3 mutated in Hermansky-Pudlak syndrome is a Rab32/38 guanine nucleotide exchange factor. *Curr. Biol.* **22**, 2135-2139.

Girard, E., Chmiest, D., Fournier, N., Johannes, L., Paul, J.-L., Vedie, B. and Lamaze, C. (2014). Rab7 is functionally required for selective cargo sorting at the early endosome. *Traffic* **15**, 309-326.

Guo, P., Hu, T., Zhang, J., Jiang, S. and Wang, X. (2010). Sequential action of *Caenorhabditis elegans* Rab GTPases regulates phagolysosome formation during apoptotic cell degradation. *Proc. Natl. Acad. Sci. USA* **107**, 18016-18021.

Horgan, C. P., Hanscom, S. R. and McCaffrey, M. W. (2013). GRAB is a binding partner for the Rab11a and Rab11b GTPases. *Biochem. Biophys. Res. Commun.* **441**, 214-219.

Huotari, J. and Helenius, A. (2011). Endosome maturation. *EMBO J.* **30**, 3481-3500.

Johansson, M., Rocha, N., Zwart, W., Jordens, I., Janssen, L., Kuijl, C., Olkkonen, V. M. and Neefjes, J. (2007). Activation of endosomal dynein motors by stepwise assembly of Rab7-RILP-p150[Glued], ORP1L, and the receptor βIII spectrin. *J. Cell Biol.* **176**, 459-471.

Kawase, K., Nakamura, T., Takaya, A., Aoki, K., Namikawa, K., Kiyama, H., Inagaki, S., Takemoto, H., Saltiel, A. R. and Matsuda, M. (2006). GTP hydrolysis by the Rho family GTPase TC10 promotes exocytic vesicle fusion. *Dev. Cell* **11**, 411-421.

Kimura, S., Noda, T. and Yoshimori, T. (2007). Dissection of the autophagosome maturation process by a novel reporter protein, tandem fluorescent-tagged LC3. *Autophagy* **3**, 452-460.

Kinchen, J. M. and Ravichandran, K. S. (2010). Identification of two evolutionarily conserved genes regulating processing of engulfed apoptotic cells. *Nature* **464**, 778-782.

Kitano, M., Nakaya, M., Nakamura, T., Nagata, S. and Matsuda, M. (2008). Imaging of Rab5 activity identifies essential regulators for phagosome maturation. *Nature* **453**, 241-245.

Komatsu, N., Aoki, K., Yamada, M., Yukinaga, H., Fujita, Y., Kamioka, Y. and Matsuda, M. (2011). Development of an optimized backbone of FRET biosensors for kinases and GTPases. *Mol. Biol. Cell* **22**, 4647-4656.

Lam, A. J., St-Pierre, F., Gong, Y., Marshall, J. D., Cranfill, P. J., Baird, M. A., McKeown, M. R., Wiedenmann, J., Davidson, M. W., Schnitzer, M. J. et al. (2012). Improving FRET dynamic range with bright green and red fluorescent proteins. *Nat. Methods* **9**, 1005-1012.

Lawrence, G., Brown, C. C., Flood, B. A., Karunakaran, S., Cabrera, M., Nordmann, M., Ungermann, C. and Fratti, R. A. (2014). Dynamic association of the PI3P-interacting Mon1-Ccz1 GEF with vacuoles is controlled through its phosphorylation by the type 1 casein kinase Yck3. *Mol. Biol. Cell* **25**, 1608-1619.

Luzio, J. P., Pryor, P. R. and Bright, N. A. (2007). Lysosomes: fusion and function. *Nat. Rev. Mol. Cell Biol.* **8**, 622-632.

Mizuno, K., Kitamura, A. and Sasaki, T. (2003). Rabring7, a novel Rab7 target protein with a RING finger motif. *Mol. Biol. Cell* **14**, 3741-3752.

Mochizuki, N., Yamashita, S., Kurokawa, K., Ohba, Y., Nagai, T., Miyawaki, A. and Matsuda, M. (2001). Spatio-temporal images of growth-factor-induced activation of Ras and Rap1. *Nature* **411**, 1065-1068.

Moreno, A., SantoDomingo, J., Fonteriz, R. I., Lobatón, C. D., Montero, M. and Alvarez, J. (2010). A confocal study on the visualization of chromaffin cell secretory vesicles with fluorescent targeted probes and acidic dyes. *J. Struct. Biol.* **172**, 261-269.

Mullock, B. M., Bright, N. A., Fearon, C. W., Gray, S. R. and Luzio, J. P. (1998). Fusion of lysosomes with late endosomes produces a hybrid organelle of intermediate density and is NSF dependent. *J. Cell Biol.* **140**, 591-601.

Nguyen, A. W. and Daugherty, P. S. (2005). Evolutionary optimization of fluorescent proteins for intracellular FRET. *Nat. Biotechnol.* **23**, 355-360.

Nordmann, M., Cabrera, M., Perz, A., Bröcker, C., Ostrowicz, C., Engelbrecht-Vandré, S. and Ungermann, C. (2010). The Mon1-Ccz1 complex is the GEF of the late endosomal Rab7 homolog Ypt7. *Curr. Biol.* **20**, 1654-1659.

Nordmann, M., Ungermann, C. and Cabrera, M. (2012). Role of Rab7/Ypt7 in organizaing membrane trafficking at the late emdosome. In *Rab GTPases and Membrane Trafficking* (ed. G. Li and N. Seqev), pp. 132-143. Sharjah: Bentham Science Publishers.

Ohba, Y., Kurokawa, K. and Matsuda, M. (2003). Mechanism of the spatio-temporal regulation of Ras and Rap1. *EMBO J.* **22**, 859-869.

Ohbayashi, N., Maruta, Y., Ishida, M. and Fukuda, M. (2012). Melanoregulin regulates retrograde melanosome transport through interaction with the RILP-p150[Glued] complex in melanocytes. *J. Cell Sci.* **125**, 1508-1518.

Poteryaev, D., Datta, S., Ackema, K., Zerial, M. and Spang, A. (2010). Identification of the switch in early-to-late endosome transition. *Cell* **141**, 497-508.

Racoosin, E. L. and Swanson, J. A. (1993). Macropinosome maturation and fusion with tubular lysosomes in macrophages. *J. Cell Biol.* **121**, 1011-1020.

Rink, J., Ghigo, E., Kalaidzidis, Y. and Zerial, M. (2005). Rab conversion as a mechanism of progression from early to late endosomes. *Cell* **122**, 735-749.

Rojas, R., van Vlijmen, T., Mardones, G. A., Prabhu, Y., Rojas, A. L., Mohammed, S., Heck, A. J. R., Raposo, G., van der Sluijs, P. and Bonifacino, J. S. (2008). Regulation of retromer recruitment to endosomes by sequential action of Rab5 and Rab7. *J. Cell Biol.* **183**, 513-526.

Saftig, P. and Klumperman, J. (2009). Lysosome biogenesis and lysosomal membrane proteins: trafficking meets function. *Nat. Rev. Mol. Cell Biol.* **10**, 623-635.

Schoebel, S., Oesterlin, L. K., Blankenfeldt, W., Goody, R. S. and Itzen, A. (2009). RabGDI displacement by DrrA from *Legionella* is a consequence of its guanine nucleotide exchange activity. *Mol. Cell* **36**, 1060-1072.

Settembre, C., Fraldi, A., Medina, D. L. and Ballabio, A. (2013). Signals from the lysosome: a control centre for cellular clearance and energy metabolism. *Nat. Rev. Mol. Cell Biol.* **14**, 283-296.

Sivars, U., Aivazian, D. and Pfeffer, S. R. (2003). Yip3 catalyses the dissociation of endosomal Rab–GDI complexes. *Nature* **425**, 856-859.

Spinosa, M. R., Progida, C., De Luca, A., Colucci, A. M. R., Alifano, P. and Bucci, C. (2008). Functional characterization of Rab7 mutant proteins associated with Charcot-Marie-Tooth type 2B disease. *J. Neurosci.* **28**, 1640-1648.

Stenmark, H. (2009). Rab GTPases as coordinators of vesicle traffic. *Nat. Rev. Mol. Cell Biol.* **10**, 513-525.

Swanson, J. A. (2008). Shaping cups into phagosomes and macropinosomes. *Nat. Rev. Mol. Cell Biol.* **9**, 639-649.

Tabata, K., Matsunaga, K., Sakane, A., Sasaki, T., Noda, T. and Yoshimori, T. (2010). Rubicon and PLEKHM1 negatively regulate the endocytic/autophagic pathway via a novel Rab7-binding domain. *Mol. Biol. Cell* **21**, 4162-4172.

Vanlandingham, P. A. and Ceresa, B. P. (2009). Rab7 regulates late endocytic trafficking downstream of multivesicular body biogenesis and cargo sequestration. *J. Biol. Chem.* **284**, 12110-12124.

Vonderheit, A., Helenius, A. and Simons, K. L. (2005). Rab7 associates with early endosomes to mediate sorting and transport of Semliki forest virus to late endosomes. *PLoS. Biol.* **3**, e233.

Waguri, S., Tomiyama, Y., Ikeda, H., Hida, T., Sakai, N., Taniike, M., Ebisu, S. and Uchiyama, Y. (2006). The luminal domain participates in the endosomal trafficking of the cation-independent mannose 6-phosphate receptor. *Exp. Cell Res.* **312**, 4090-4107.

Wang, C.-W., Stromhaug, P. E., Shima, J. and Klionsky, D. J. (2002). The Ccz1-Mon1 protein complex is required for the late step of multiple vacuole delivery pathways. *J. Biol. Chem.* **277**, 47917-47927.

Wang, T., Liu, Y., Xu, X.-H., Deng, C.-Y., Wu, K.-Y., Zhu, J., Fu, X.-Q., He, M. and Luo, Z.-G. (2011). Lgl1 activation of rab10 promotes axonal membrane trafficking underlying neuronal polarization. *Dev. Cell* **21**, 431-444.

Wartosch, L., Bright, N. A. and Luzio, J. P. (2015). Lysosomes. *Curr. Biol.* **25**, R315-R316.

Yousefian, J., Troost, T., Grawe, F., Sasamura, T., Fortini, M. and Klein, T. (2013). Dmon1 controls recruitment of Rab7 to maturing endosomes in *Drosophila*. *J. Cell Sci.* **126**, 1583-1594.

Yusa, K., Rad, R., Takeda, J. and Bradley, A. (2009). Generation of transgene-free induced pluripotent mouse stem cells by the piggyBac transposon. *Nat. Methods* **6**, 363-369.